Thermochimica Acta, 171 (1990) 193–206
Elsevier Science Publishers B.V., Amsterdam

A THERMOGRAVIMETRIC STUDY OF COAL DECOMPOSITION UNDER IGNITION CONDITIONS

M.A. SERAGELDIN *
EBT International, P.O. Box 25065, Winston-Salem, NC 27114-5065 (U.S.A.)

HAI WANG *
Fuel Science Program, Materials Science and Engineering Department, Pennsylvania State University, University Park, PA 16802 (U.S.A.)

(Received 28 March 1990)

ABSTRACT

Three coals of high volatility, PSOC-24 (bituminous), PSOC-240A (sub-bituminous) and PSOC-1430p (lignite), have been decomposed using a Du Pont 951 thermogravimetric analyzer. A gas flow of pure oxygen was maintained during each run. The experiments were performed under a wide range of heating rates, using two different heating modes (isothermal and programming). The ignition temperature of a coal sample was found to increase with sample mass. A minimum occurred as the heating rate was increased from 10 to 800 °C min^{-1}. The activation energy of ignition was 28 kJ mol^{-1} for heating rates < 50 °C min^{-1} and 18.2 kJ mol^{-1} in the higher heating rate region (50–800 °C min^{-1}). This would suggest that ignition occurred by different mechanisms in the different heating rate regions. The rate of devaporization increased with sample heating rate and moisture content of the coal samples. A relationship was found between the burning-rate constants of the devolatilization and char burn-out stages and the heat release rates during combustion. The burning rates of the coals were ordered as follows: PSOC-1430p > PSOC-240A > PSOC-24. This relationship is consistent with the porosity and calcium levels of the coal samples.

INTRODUCTION

Decomposition profiles of coal samples have been studied extensively by differential thermogravimetric analysis (DTG) in both pyrolytic and oxidative environments [1–7]. Such profiles are empirical in nature, since they depend on experimental conditions such as sample size, furnace temperature and design. However, they have been used with some success to evaluate the

* This work was carried out when both authors were at the Department of Chemistry and Chemical Engineering, Michigan Technological University, Houghton, MI 49931, U.S.A.

0040-6031/90/$03.50

performance of coal under specific furnace conditions. This is partly due to the existence of a correlation between the rank of coal and the general shape of the DTG burning profile [1–3]. However, there is a disadvantage associated with the DTG burning profile method in analysis of coals of high volatility, such as lignite. Interpretation of the profiles is difficult because of overlapping of several devolatilization peaks.

We have previously reported results of studies of polymer ignition and combustion using a thermogravimetric analyzer (TGA) [8–10]. The same technique was used in the present work to study the decomposition profiles of three well characterized coals of high volatility. Because of the importance of sample heating rate, its effect on the burning behavior was investigated. The kinetics of the devaporization, devolatilization and char burn-out stages was also studied, using several models. These included the contracting area/volume models, the unimolecular decay law, and several Avrami–Erofeev-type equations. An equation of this last type has been found to be suitable for studying coal. Vernekar et al. [11] investigated the effect of coal pellet density on the rate of oxidative decomposition of coal using TGA.

EXPERIMENTAL

Materials

Three coals of high volatility, PSOC-24 (highly volatile bituminous), PSOC-240A (sub-bituminous) and PSOC-1430p (lignite), were obtained from the Pennsylvania State University coal bank. The samples were size-reduced from about 6 mm (1/4 inch) to produce 270 mesh particles, and stored in glass vials. Results of proximate and ultimate analyses of the coals are given in Table 1. The surface areas and porosities of the coal samples, measured using a Micromeritics porosimeter (Autopore 9200), are also listed in Table 1. The mineral compositions of the coal samples (Table 1) were obtained using a scanning electron microscope (SEM) analyzer combined with an energy-dispersive X-ray analyzer. A JOEL Model JSM-35C SEM interfaced with a Kevex Analyst and an 8000 Microanalyzer was used. Details of the procedures followed can be found elsewhere [12].

Micrographs for the three coal samples obtained using the SEM analyzer are shown in Fig. 1. The surface of the PSOC-24 particles was nearly flat, with only a few open pores. PSOC-1430p had the largest open pores, while those of the PSOC-240A sample were intermediate in size between those of the other two coals.

Apparatus and procedures

Decomposition measurements were performed using a Du Pont 951 thermogravimetric analyzer controlled by a Du Pont 910 unit. A small

TABLE 1

Characteristics of the coals used

	PSOC-24	PSOC-240A	PSOC-1430p
Proximate analysis (wt.%)			
% Moisture	5.04	8.74	8.75
% Volatile matter	35.43	38.92	41.70
% Fixed carbon	52.53	37.30	38.82
% Ash	7.00	15.04	10.73
Ultimate analysis (wt.%) dry-ash free basis			
C	67.19	57.35	61.18
H	5.09	4.84	4.44
O	27.72	37.81	34.38
Heat content (BTU hr^{-1})	14090	13680	13030
Mineral matter analysis (wt.%)			
Na	–	–	6.13
Mg	–	–	3.65
Al	4.33	9.95	4.48
Si	7.22	22.10	15.03
S	20.68	5.51	9.23
K	0.80	0.47	0.71
Ca	0.73	7.94	9.18
Ti	–	1.03	–
Fe	13.17	2.40	1.39
Cu	4.64	2.94	5.22
O	48.43	47.66	44.98
Density, total pore volume and porosity			
Density (g cm^{-3}): He	1.41	1.54	1.51
Density (g cm^{-3}): Hg	0.84	1.00	0.85
Porosity (%)	40.4	35.2	43.7
V_{total} (cm^3 g^{-1})	0.481	0.352	0.514
V_{macro} (cm^3 g^{-1})	0.222	0.142	0.438
V_{micro} (cm^3 g^{-1})	0.259	0.210	0.076
$S_{internal}$ (m^2 g^{-1})	446.0	378.0	137.0

sample of coal (2.5–10.5 mg) was spread evenly onto the TGA platinum sample pan to reduce the effect of sample shape. The oxidant stream was pure oxygen flowing at 50 ml min^{-1}. The temperature was monitored by a thermocouple positioned on one side of the sample pan, about 5 mm from its center.

The effect of initial sample mass on the ignition characteristics was investigated using 2.5, 5.0 and 10.5 mg of coal, at an isothermal furnace temperature of 800 °C. To study the effect of heating rate on the ignition and combustion stages, a sample of about 10.5 mg was used.

The instrument was operated under two modes to achieve the desired range of sample heating rates. In the programming mode, the quartz tube

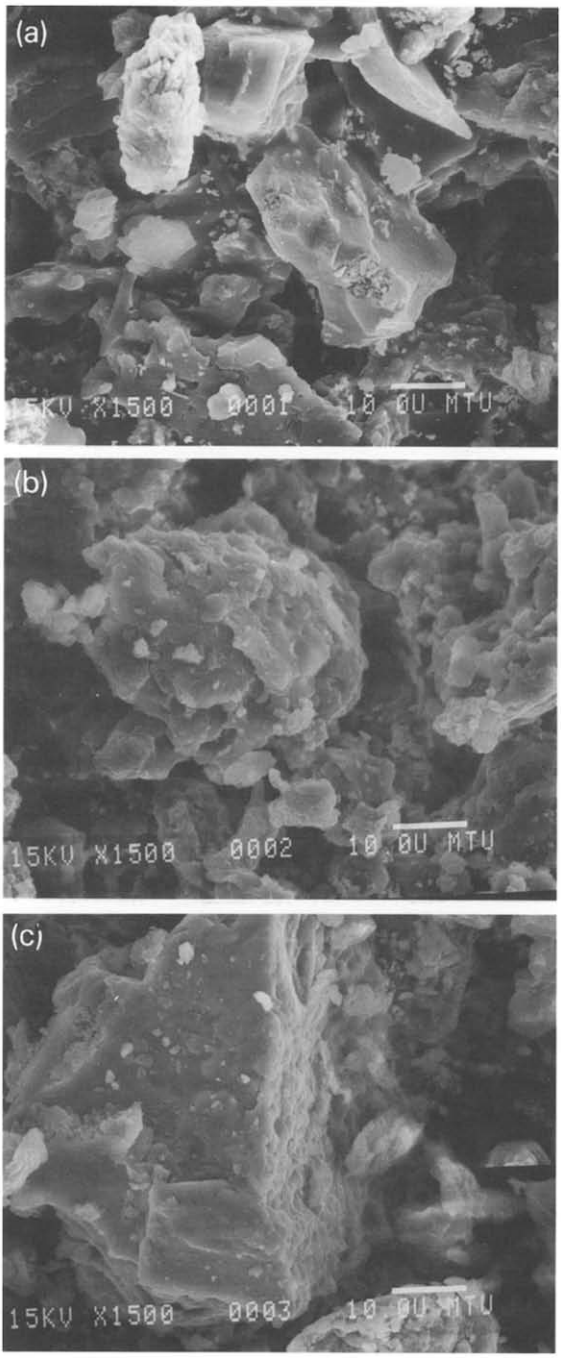

Fig. 1. SEM micrographs of the coal samples: a, PSOC-24; b, PSOC-240A; c, PSOC-1430p.

and sample-balance system were placed inside the TGA furnace before the heating cycle was begun. This mode provided a low range of heating rates, 10–100 °C min^{-1}. Higher heating rates, from 200 to 800 °C min^{-1}, were

obtained by running the system in the isothermal mode. Before every run, the furnace was left to equilibrate at the pre-set temperature for 5 min. The quartz tube and sample-balance system were then rapidly introduced into the pre-heated TGA furnace using a pneumatic driver.

RESULTS

Typical TG curves for coal in the isothermal mode are shown in Fig. 2. The ignition temperature T_{ig} was determined at the point where the temperature–time curve underwent a sudden rise. This is illustrated for the case when the furnace temperature was set at 400 °C. Three stages of decomposition can be identified. Stage I was due to loss of absorbed moisture (devaporization), while Stages II and III were due to devolatilization and char burn-out, respectively. The effect of sample mass on the ignition temperature is shown in Fig. 3. Evidently, T_{ig} increased with initial sample mass.

The shape of the TGA curves was not much different from those obtained during polymer ignition [8–10], except that for coal (the present study), the temperature–time relationship was always fairly linear. As a result, the sample heating rate of a run in isothermal mode can be calculated from the relationship

$$H_r = (T_{ig} - T_i)/(t_{ig} - t_i) \tag{1}$$

where H_r is the heating rate, T_{ig} the ignition temperature, T_i the room temperature (≈ 23 °C), t_{ig} the time to ignition, and t_i the initial time.

In the higher heating rate region, i.e. 200–800 °C min^{-1}, the isothermal furnace temperature T_{iso} and heating rate data were regressed. This resulted in the useful relationship

$$T_{iso} = T_i + \alpha H_r^{\frac{1}{2}} \qquad r^2 = 0.999 \tag{2}$$

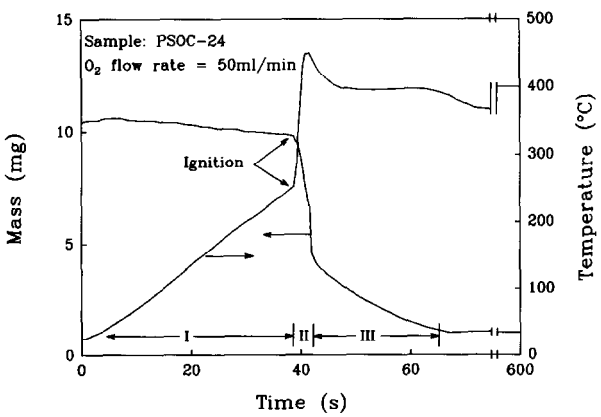

Fig. 2. Typical TG curves of coal decomposition, ignition and combustion at $T_{iso} = 400$ °C.

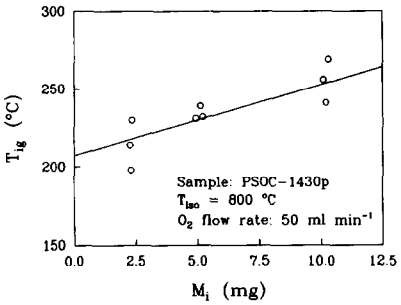

Fig. 3. Effect of initial sample mass on ignition temperature.

T_i and α were found to be 22.8 °C and 20.0 °C$^{1/2}$ min$^{1/2}$, respectively. The value of T_i in eqn. (2) was very close to the room temperature, which supports the adequacy of this equation. (T_{iso} is expected to be equal to the room temperature T_i when the heating rate is 0 °C min^{-1}.)

The dependence of T_{ig} on H_r is shown in Fig. 4. At this point it is not possible to explain why T_{ig} first decreased with heating rate and then increased when H_r was greater than 50 °C min^{-1}. However, this pattern may indicate that the mechanism of decomposition in the two regions is not the same. The mass loss of the coals before ignition exceeded by less than 3% the moisture content determined from proximate analysis (ASTM, Table 1). This small difference can be attributed to the use of two different techniques (i.e. TG and ASTM), and is not sufficient cause to rule out the occurrence of heterogeneous ignition.

It was also found, in contrast to the results for polymers [8–10], that there was no low heating rate limit for coal below which ignition could not occur. This can be deduced from Fig. 5, which is a plot of the reciprocal of time-to-ignition against heating rate, up to 100 °C min^{-1}. For each coal sample, the experimental points fell fairly close to a straight line through the origin.

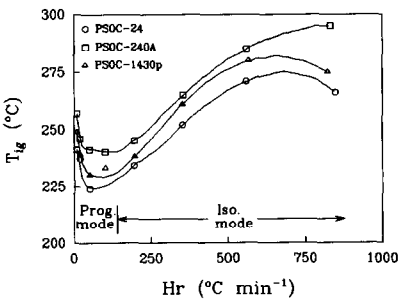

Fig. 4. Effect of sample heating rate on ignition temperature.

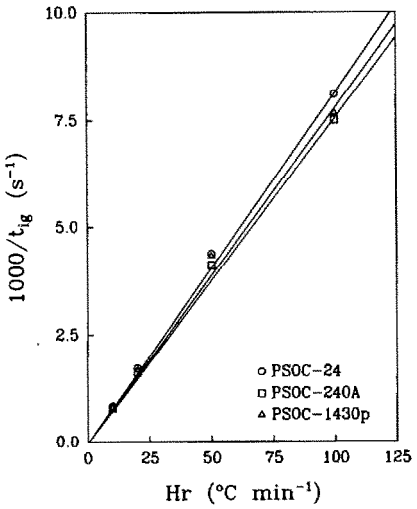

Fig. 5. Effect of heating rate on the time to ignition.

Activation energy of ignition

The following kinetic equation was used to determine the activation energy of ignition E_{ig}:

$$1/t_{ig} = A \exp(-E_{ig}/RT_{isoKE}) \quad (3)$$

where t_{ig} is the time to ignition (in s), A the pre-exponential factor (in s^{-1}), R the universal gas constant (in kJ mol^{-1} K^{-1}), and T_{isoKE} the isothermal furnace temperature (in K).

The time it takes for coal particles to ignite is dependent on the gas environment, the size of the coal particles and the properties of the coal surface. The particle size distribution was designed to be the same, to remove this effect. However, when the isothermal mode is used, variations in sample distribution on the sample pan, or in sample mass, will affect the sample heating rate [9–10]. This in turn will affect the value of t_{ig} corresponding to a given isothermal run. Therefore, a corrected (or effective) isothermal furnace temperature T_{isoKE} was calculated, by substituting into eqn. (2) the sample heating rate measured for an isothermal run. For the programming runs, where the heating rates ranged from 10 to 100 °C min^{-1}, T_{isoKE} was obtained by substituting the programmed heating rate into eqn. (2). In this case, T_{isoKE} should be understood to be the isothermal furnace temperature which would result in the corresponding programmed heating run. The temperature values less than 440 K in Fig. 6 ($1/T_{isoKE} \geq 2.3 \times 10^{-3}$ K^{-1}) correspond to the TGA set heating rates less than or equal to 100 °C min^{-1}.

As shown in Fig. 6, the data fell on two distinct straight lines connected at point 'a': one for the low heating rates (II) and the other for the high

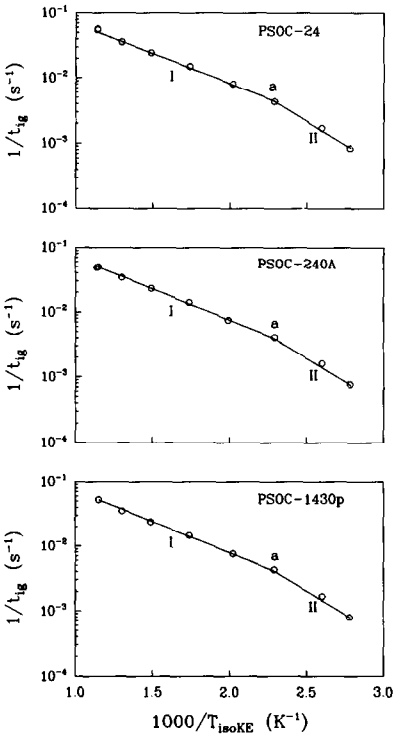

Fig. 6. Activation energies of ignition.

heating rates (I). Since the heating rate at that point was not 100 °C min^{-1} but close to 50 °C min^{-1}, this was not an effect of using two different operating modes. The slopes of the lines meeting at point 'a' provide a measure of the (procedural) ignition activation energies in these two regions.

The ignition rate parameters are listed in Table 2. The activation energy E_{ig} was about 28 kJ mol^{-1} in the low heating rate region and 18.2 kJ mol^{-1} in the high heating rate region, for all three coal samples. This evidence suggests that the rate-controlling mechanism leading to ignition is not the same in the two regions. It also explains the minimum obtained in Fig. 4 at 50 °C when T_{ig} was plotted against H_r. In the high heating rate region, the

TABLE 2

Activation energies of ignition

E_{ig} (kJ mol^{-1}) [a]	10–50 °C min^{-1}		50–800 °C min^{-1}	
	A (s^{-1})	E_{ig} (kJ mol^{-1})	A (s^{-1})	E_{ig} (kJ mol^{-1})
PSOC-24	8.50	27.5 ± 1.8	0.670	18.3 ± 0.3
PSOC-240A	8.41	27.6 ± 2.0	0.609	18.2 ± 0.2
PSOC-1430p	9.52	28.1 ± 1.9	0.647	18.2 ± 0.3

[a] ± One standard deviation.

ignitability of these coals can be characterized by the value of the pre-exponential factor, $A_{\text{PSOC-24}} > A_{\text{PSOC-1430p}} > A_{\text{PSOC-240A}}$. This follows the same trend as that in Fig. 4; that is, the lower the ignition temperature, the higher the pre-exponential factor. In the low heating rate region, there was no significant trend. This range was represented by only three heating rates.

Coal reactivity

Both the generalized Avrami–Erofeev equation ($n = 2$, 3, 4) and the unimolecular decay law ($n = 1$) were selected for coal reactivity analysis. These equations may be represented by the following general form [13]

$$[-\ln(1 - C)]^{1/n} = k(t - t_0) \tag{4}$$

where C is the weight fraction converted. The power index n can therefore take whole digit values from one to four. Also tested was the contracting area/volume model

$$[1 - (1 - C)]^{1/n} = k(t - t_0) \tag{5}$$

where n equals one/two. Because the above models are empirical for organic solids, it is not possible to predict which of the equations discussed above gives the best representation of the data for the three decomposition regions. In the following sections the coal reactivities in the three decomposition stages shown in Fig. 2 are compared, and the suitability of the models is discussed.

Plots of $[-\ln(1 - C)]^{1/n}$ and $[1 - (1 - C)]^{1/n}$ against t for all three coal samples at $T_{\text{iso}} = 500\,^{\circ}\text{C}$ are shown in Fig. 7. In each case, the three decomposition stages, devaporization, devolatilization and char burn-out, defined by the TGA mass loss curve in Fig. 2, are clearly distinguishable.

It was decided, however, not to use eqn. (4) with n ranging from 2 to 4 for the kinetic studies, because of the high curvature produced in the devaporization region (Stage I). When eqn. (4) with $n = 1$ (also known as the unimolecular decay law) and the contracting area/volume model (eqn. (5)) were compared, it was found that the lines in all three decomposition stages were about equally linear in every case. The lines close to the transition point, from the end of the devolatilization region (Stage II) to the char burn-out region (Stage III), were more linear when the unimolecular decay model was used, resulting in a higher regression coefficient. It was for this reason that eqn. (4) with $n = 1$

$$-\ln(1 - C) = k(t - t_0) \tag{6}$$

was chosen to determine the kinetic constants in the present study. The rate coefficient k was obtained by applying linear regression to the data in terms of $-\ln(1 - C)$ and t. The correlation coefficient r was always above 0.95.

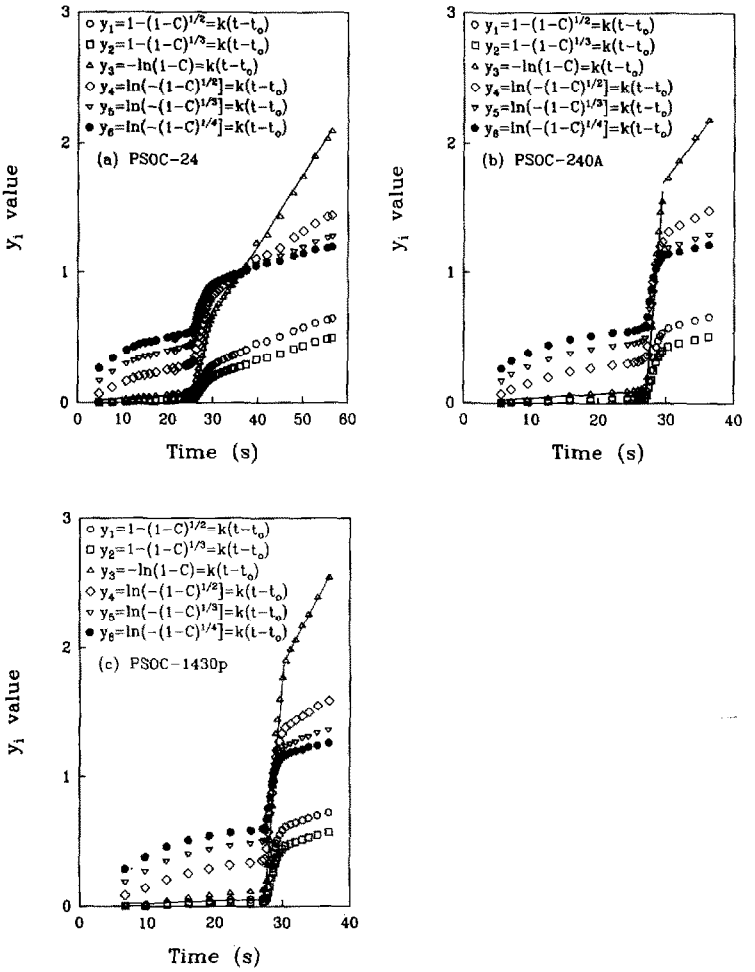

Fig. 7. Comparison of goodness of fit using various kinetic models at $T_{iso} = 500\,^{\circ}C$: a PSOC-24; b, PSOC-240A; c, PSOC-1430p.

The rate constant in the devaporization stage k_I was found to increase with isothermal furnace temperature T_{iso} (which determined sample heating rate) and coal moisture content (Fig. 8). In Stages II and III, which represented the devolatilization and char burn-out stages, the rate coefficients (k_{II} and k_{III}) followed the order

PSOC-1430p (lignite) > PSOC-240A (sub-bituminous)
> PSOC-24 (bituminous)

In Figs. 9 and 10 the rate coefficients in the aforementioned two stages are shown plotted against the average rate of temperature rise during ignition $(\Delta T/\Delta t)_{ig}$. The ratio $(\Delta T/\Delta t)_{ig}$ may be considered to be a measure of the heat release rate during ignition. Hence

$$Q \propto (\Delta T/\Delta t)_{ig} = (T_{max} - T_{ig})/(t_{max} - t_{ig}) \quad (7)$$

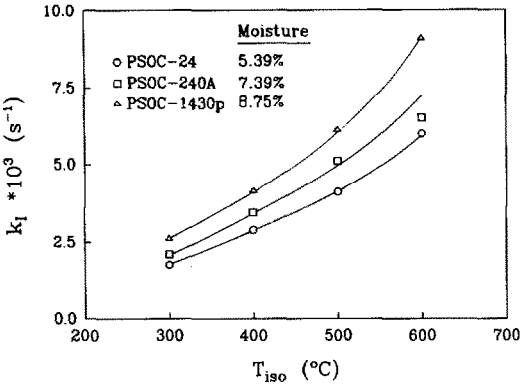

Fig. 8. Effect of isothermal furnace temperature and moisture content on the devaporization rate.

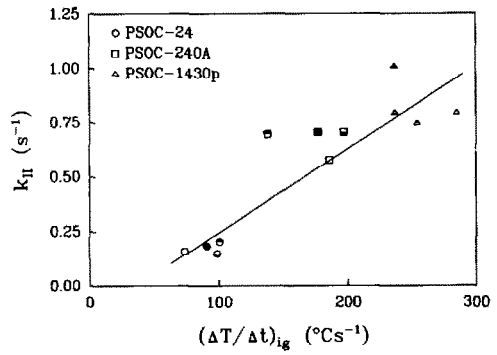

Fig. 9. Relationship between the average temperature rise rate at ignition and the rate coefficient in the devaporization stage; symbols unfilled, $T_{iso} = 300\,°C$; upper half filled, $T_{iso} = 400\,°C$; lower half filled, $T_{iso} = 500\,°C$; filled, $T_{iso} = 600\,°C$.

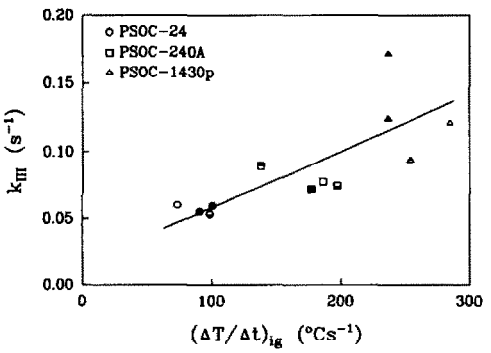

Fig. 10. Relationship between the average temperature rise rate at ignition and the rate coefficient in the char burn-out stage; symbols unfilled, $T_{iso} = 300\,°C$; upper half filled, $T_{iso} = 400\,°C$; lower half filled, $T_{iso} = 500\,°C$; filled, $T_{iso} = 600\,°C$.

where T_{max} is the peak temperature on a TGA curve and t_{max} is the corresponding time when the peak appears. Both k_{II} and k_{III} increased with heat release rate. This suggested that the rate coefficient k obtained using the unimolecular decay law was an appropriate indicator of the coal reactivity under the conditions used in the present study. In Figs. 9 and 10 each cluster of points (with the same symbol) represents data at several isothermal furnace temperatures, between 300 and 600 °C. Since the position of the points within a cluster was random, one may deduce that the burning rate in both decomposition stages, II and III, was not affected by the isothermal furnace temperature.

DISCUSSION

It has been suggested that the ignition temperature decreases as the volatile matter content of coal increases [14]. This general rule did not work well when applied to coals of high volatility. The ignition temperature did not show any trend with the volatile matter content (Table 1) of the three coal samples. On the basis of the volatile matter content, the ignition temperature of the coals should follow the order

PSOC-1430p (lignite) > PSOC-240A (sub-bituminous)
> PSOC-24 (bituminous)

However, the ignition temperatures measured in the present study consistently followed the order

PSOC-24 < PSOC-1430p < PSOC-240A

The combustion rate in the devolatilization and char burn-out stages followed a trend based on coal rank, i.e. lignite coal had the highest rate of the three, and bituminous coal the lowest.

The burning rate of a coal is also dependent on the accessibility of the oxidant to the coal active sites, which points to the importance of pore size distribution. Another parameter is coal mineral content, i.e. the nature and distribution of the minerals in the coal. Results in Table 1 show that PSOC-1430p had the largest macro-pore volume and smallest internal surface area of the three coals. PSOC-24 had the smallest macro-pore volume and largest internal surface area. Although the burning rate in regions II and III followed the same order as the macro-pore volume, one cannot assume that the latter parameter, evaluated at room temperature, is the major factor determining the reactivity of a coal throughout the burning stage.

A more important factor, in this case, is the difference in composition and distribution of the minerals in these coals. PSOC-24 contained a significantly smaller amount of calcium than the other two coals (0.73% for PSOC-24, 7.94% for PSOC-240A and 9.23% for PSOC-1430p). Calcium is an

important mineral matter which can promote reactivities of both coal and char [12,15]. Therefore, the lower burning rate of PSOC-24 may be mainly attributable to a low amount of calcium in the coal. The higher reactivity of the lignite coal may also be attributable to the presence of significantly higher amounts of magnesium and sodium, which have catalytic properties. Calcium is likely to be evenly distributed in lignite [12].

In this study, the unimolecular decay law was adopted for kinetic analysis of the coal data based on the regression results; whereas in a previous study [10], of the rate of oxidative decomposition and combustion of thermoplastic polymers, using $n = 4$ in the Avrami–Erofeev-type equation gave the best representation of the experimental data. In both cases, three main decomposition stages were identifiable on each thermogram. There were, however, a number of differences. The polymers melted before decomposing, and one can therefore state that the reaction was of the gas–liquid type; whereas in the case of coal it was of the gas–solid type. In the polymer runs, the TGA balance recorded a significant mass loss ($> 7\%$) before the occurrence of ignition in the gas phase. For coal it was not possible to resolve the position of ignition because only a small mass loss was detected then. Having said that, one should not place too much significance on the difference in the values of the power index n in eqn. (4) of this study.

CONCLUSIONS

(1) The mechanism of ignition was different at low ($\leqslant 50\,^{\circ}\mathrm{C\ min^{-1}}$) and high ($\geqslant 100\,^{\circ}\mathrm{C\ min^{-1}}$) heating rates. This was indicated by a difference in the activation energy of ignition.

(2) The combustion rate for the devolatilization and char burn-out stages was related to both the open pores and the amount and distribution of calcium and other important minerals present in the coal samples.

(3) A model of the type $[-\ln(1 - C)]^{1/n} = k(t - t_0)$ may be used for studying samples that exhibit multiple decomposition stages. However, the unimolecular decay law (i.e. $n = 1$) is recommended for gas–solid reactions.

REFERENCES

1 C.L. Wagoner and A.F. Duzy, ASME Publication 67-WA/FU-4, 1967.
2 C.L. Wagoner and E.C. Winegartner, J. Eng. Power, April (1973) 119.
3 J.W. Cummings and J. McLaughlin, Thermochim. Acta, 57 (1982) 253.
4 C.H. Saayman, Thermochim. Acta, 93 (1985) 369.
5 P. Ghetti, U.D. Robertis, S.D. Antoine, M. Villani and. E. Chiellini, Fuel, 64 (1985) 950.
6 A. DeKoranyi, Thermochim. Acta, 110 (1987) 527.
7 S.E. Smith, R.C. Neavel, E.J. Hippo and R.N. Miller, Fuel, 60 (1981) 258.

8 M.A. Serageldin and H. Wang, Proc. 1986 Nat. Conf. of Standards Laboratories, Gaithersberg, MD, October 6–9, National Conference of Standards Laboratories, Boulder Co. Vol. 1, Technical Presentation, pp. 8.1–8.13.
9 M.A. Serageldin and H. Wang, Thermochim. Acta, 117 (1987) 157.
10 M.A. Serageldin and H. Wang, Thermochim. Acta, 125 (1988) 247.
11 V.R.P. Vernekar, J.R.M. Rao, B.K.S. Rao and M.A. Tirunarayanan, Fuel, 61 (1981) 634.
12 W.P. Pan and M.A. Serageldin, Fuel Proc. Technol., 15 (1987) 397.
13 C.E.H. Brawn, in W.E. Garner (Ed.), Chemistry of the Solid State, Butterworth, London, 1955, p. 254.
14 D.W. van Krevelen and J. Schuyer, Coal Science: Aspects of Coal Constitution, Elsevier, New York, 1957, Chap. 15, p. 312.
15 W.P. Pan and M.A. Serageldin, Thermochim. Acta, 125 (1988) 285.